Characteristics of Acoustic Standing Waves in Fluidized Beds

C. A. Herrera and E. K. Levy
Energy Research Center, Lehigh University, Bethlehem, PA 18015

J. Ochs
Dept. of Mechanical Engineering and Mechanics, Lehigh University, Bethlehem, PA 18015

Fine particles are typically difficult to fluidize with gas, due to interparticle forces that cause the bed material to be cohesive. The use of acoustic waves, generated by a loudspeaker positioned above the bed, to agitate the bed material and enhance fluidization, has been investigated. The bed was fluidized with air at conditions near minimum bubbling. Sound-pressure measurements within the bed showed the presence of acoustic standing waves throughout the bed. Acoustic standing-wave theory, which assumes that the bed behaves as a 1-D, quasi fluid with constant speed of sound, was used to model the sound-pressure-level data. It was found that the parameter kh, where k is the wave number and h is the bed depth, determines the sound-pressure amplitude throughout the bed. The system reaches its highest sound pressure at resonance conditions for kh = (2n − 1)π/2. A comparison indicates good agreement between the theory and the experimental data.

Introduction

Fine powders, which belong to the Geldart C-Cohesive group, are usually very difficult to fluidize because their cohesiveness causes agglomeration, and channels appear (Geldart, 1973; Abrahamsen and Geldart, 1980). (Various techniques have been proposed to improve the quality of fluidization. These techniques include mechanical and centrifugal vibrations (Massimila et al., 1966; Malhotra et al., 1984; Beckmans and Chu, 1987), pulsating magnetization of magnetizable particles (Jaraiz et al., 1983; Analdos et al., 1985), and acoustic fields (Morse, 1955; Chirone et al., 1993; Chirone and Massimila, 1994).

Several articles that describe fluidization using sound-assisted chambers have been published (Chirone et al., 1993; Nowak et al., 1993; Levy et al., 1998, 1999; Herrera and Levy, 1999). In general it has been observed that high-intensity acoustic fields enhance the fluidization of fine powders, which otherwise cannot be fluidized.

No great difference in coarse-particle fluidization ($d_p > 400$ μm, Geldart group B powders) is observed when high amplitude and low-frequency sound is applied. However, fine-powder fluidization (Geldart C and A powders) has shown different behavior in the presence of a high-intensity acoustic field. The difference between coarse- and fine-particle behavior is mainly due to cohesive forces. Fine particles adhere to one another because of agglomerating forces and van der Waals forces. The agglomerating force is due to the presence of a liquid surface tension among particles. The van der Waals force is an attractive force between particles, due to variations in the local electric field contained in the solid. The van der Waals force, F_v, between two small spheres of similar diameter can be expressed as

$$F_v = \frac{L_w d_p}{32\pi z^2} \tag{1}$$

where L_w is the Lifshitz–van der Waals constant, whose value depends upon the particle properties; z is the distance of separation between the spheres; and d_p is the particle diameter.

Correspondence concerning this article should be addressed to E. K. Levy.
Current address of C. A. Herrera: Universidad del Valle, Escuela de Ingenieria Mecanica, AA 25360, Cali, Colombia.

Acoustic fields were used by Morse (1955) to improve the quality of fluidization. More recently, Chirone et al. (1992) used sound to obtain bubble-free fluidization in a fine powder of 11 μm mean particle diameter. A loudspeaker located above the bed generated the acoustic field. The sound frequency was 120 Hz, and the sound pressure level, measured above the free bed surface, ranged from 100 to 140 dB. To explain the sound effect on fluidization behavior, they proposed that the bed contains clusters of particles. Those clusters are formed by subclusters, which are groups of particles held together by van der Waals forces. The sound exerts an external force on the clusters sufficiently strong to break them apart into subclusters, but not necessarily strong enough to break up subclusters. Due to sound, the powder becomes a new pseudoparticle powder exhibiting subcluster properties, thus changing its fluidization characteristics. In a subsequent publication the same authors (Chirone et al., 1993) presented a theory to model cluster breakage. They assumed the clusters were rigid bodies made of spheres. When an external force generated by the sound overcomes the interparticle attraction force, the cluster is broken up. Chirone and Massimila (1994) extended experiments to several powders with mean particle size ranging from 0.16 μm to 11 μm. Afterwards, Chirone and Russo (1995) presented an alternate elastic model, in which breakage of the clusters occurred at certain frequency conditions. Chirone et al. (1995) published a full theoretical model. The results were presented for several conditions of bed mass, sound-pressure level at the free surface, and frequencies between 30 and 1,000 Hz. They measured the minimum fluidization and terminal velocities, and used the hydrodynamic model to obtain a corresponding hypothetical particle size that matched both velocities. The hypothetical subcluster size obtained using their model and the diameter size obtained by hydrodynamic models were compared and, in general, showed similar trends. They also found that the useful range of frequencies lay between 110 and 140 Hz, and channeling occurred above and below those limits, as well as when the sound-pressure level was lower than 130 dB. In summary, the sound affects mean particle size, changing the powder fluidization characteristics.

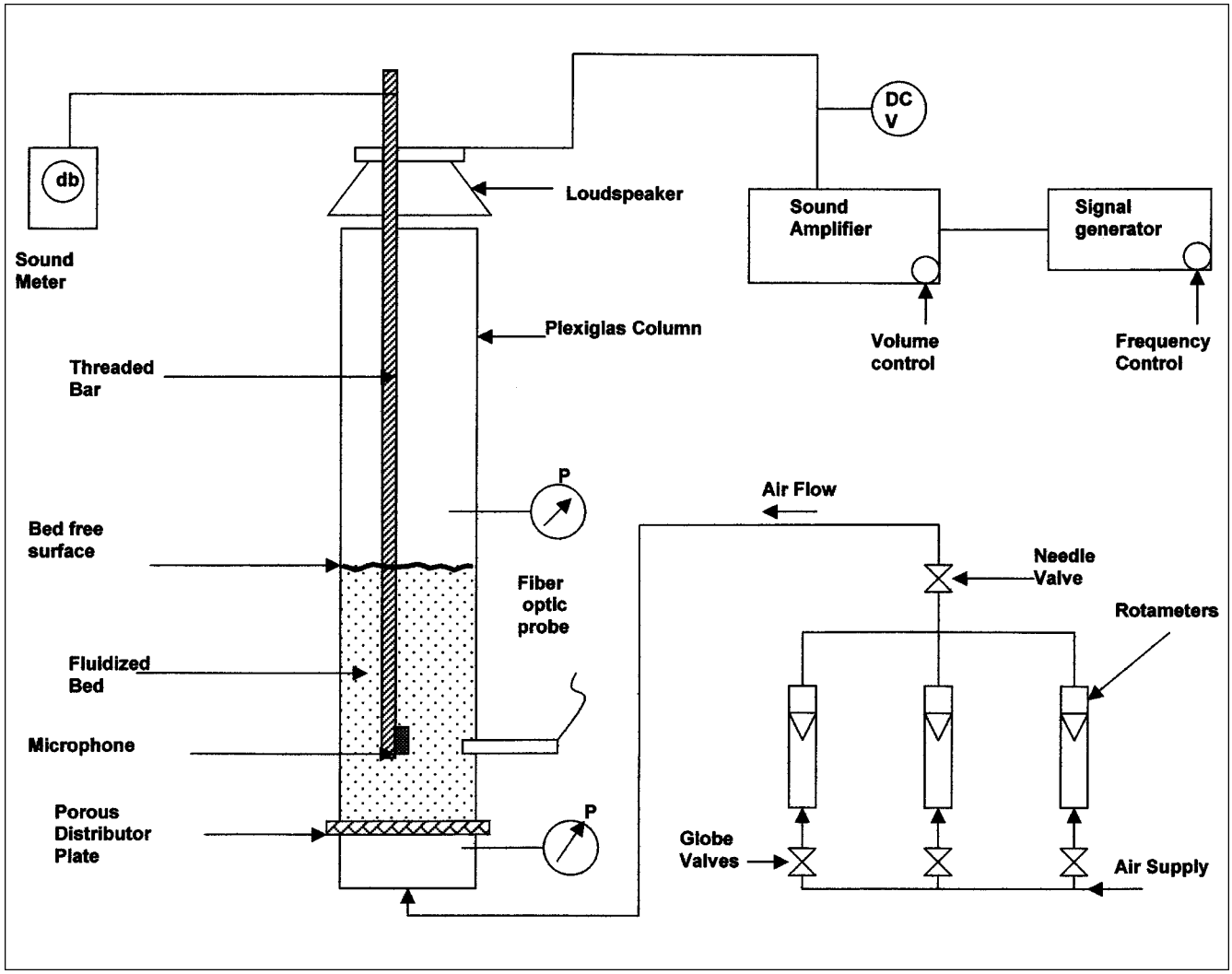

Figure 1. Laboratory apparatus.

The importance of sound-pressure level, sound frequency, and bed depth for fine-powder fluidization have been observed (Levy et al., 1999; Russo et al., 1995). All of these factors are somehow related to the sound effect on powder fluidization. However, no results have been reported on the effects of powder properties, bed geometry, or sound frequency on the sound-wave patterns in a fluidized bed. Related phenomena include acoustic resonance and attenuation; and an understanding of the governing relationships is needed in determining maximum possible sound-pressure levels and in interpreting results of fluidization experiments.

The purpose of the present investigation was to identify the parameters that control the effect of sound on fluidization, and hence to determine to what extent they influence the acoustics of the bed. The hypothesis for acoustic characterization pursued in the present work is that the fine-powder fluidized bed behaves as a quasi fluid. Therefore, the bed is treated as a single homogeneous medium, with properties that are proportional to the volume ratio of the solid and gas phases. Dynamic changes are all one-dimensional.

Experimental Apparatus and Measurement Methods

The experimental apparatus is shown in Figure 1. The sound source includes a signal generator, a sound amplifier, and a low-frequency loudspeaker. The signal generator was used to produce electric pulses with square form, whose frequency can be controlled manually with less than 1% distortion. The loudspeaker converted the signal into a sinusoidal sound wave. In most cases, the loud speaker was operated at power levels between 50 and 100 W. Experiments were performed at room temperature and atmospheric-pressure conditions.

The fluidization device consisted of a 0.15-m. ID clear Plexiglas column with a height of 0.9 m. A porous sintered glass plate located at the very bottom of the column distributed the air into the bed.

The sound-pressure-level measuring system included a microphone attached to a threaded bar tip and an audio-measuring amplifier. The microphone was a Brüel & Kjaer type 4133. The sound meter was a Brüel & Kjaer type 2609, with 170-dB maximum pressure and ± 0.3-dB precision.

The powders used in this research were mainly fly ash from two different coal power plants, labeled A and B. Fly ash B had a 40-μm mean particle size and 2-g/cm^3 particle density. Fly ash A had been sieved and the $+325$ mesh fraction was used in these experiments. Other powders used were glass beads and alumina, with sizes ranging between 1.4 μm to 80 μm and densities ranging between 1.1 and 3.95 g/cm^3.

Theory of Acoustic Standing Waves in Fluidized Beds

When a medium is dynamically disturbed, its pressure, velocity, density, and temperature change. Moreover, if the perturbation oscillates with small amplitude in a compressible fluid, the result is called a sound wave or an acoustic wave. Assuming that the acoustic propagation is an adiabatic one-dimensional process, the wave equation, written in terms of pressure, is given by the following equation (Reynolds, 1981)

$$\frac{\partial^2 p}{\partial x^2} = \frac{1}{c^2}\frac{\partial^2 p}{\partial t^2} \tag{2}$$

where p is the pressure, c is the speed of sound of the medium, t is time, and x is the axial coordinate of the wave propagation.

This equation has a known solution of the form

$$p(x,t) = Ae^{-j(\omega t - kx)} \tag{3}$$

where k is the wave number, $k = \omega/c$, which can be expressed as $k = 2\pi f/c$, or in terms of wavelength, λ, by $k = 2\pi/\lambda$; A is a constant that depends on boundary conditions; and ω is the angular frequency.

The problem that is treated in this investigation involves sound transmission in two single-phase media, confined in a vertical cylindrical vessel, with one open end and a rigid boundary at the other end. The sound source is located at the open end in the air medium. The heavier medium is the fluidized bed, which is supported by a rigid porous distributor plate. Accordingly, the media are subject to changes as the acoustic waves pass through each medium. The perturbation generated by the sound source first travels through the air. This incident pressure wave, p_{i1}, reaches the interface between the air and the fluidized bed. A fraction of the incident energy is reflected, p_{r1}, and the rest, p_t, is transmitted downward through the fluidized bed toward the distributor. Once the incident wave, p_i, reaches the distributor, a reflected wave, p_r, appears. Figure 2 depicts the acoustic waves in the fluidization column. Their effect is additive, forming a steady wave referred to as a "standing wave" (Beranek, 1996; Morse and Ingard, 1986).

The fractions of the incident-wave energy that are reflected and transmitted at an interface depend on the acoustic impedances of both media. For equal impedances, the wave is not affected by the interface, and all of the energy is transmitted forward.

The total pressure within the fluidized bed can be expressed as the sum of the incident and reflected waves (Kinsler and Frey, 1962)

$$p(x,t) = Ae^{j(\omega t + kx)} + Be^{j(\omega t - kx + \theta)} \tag{4}$$

For real values, the amplitude of Eq. 4, $|p(x,t)|$, can be written as

$$|(px,t)| = \sqrt{(A+B)^2\cos^2\left(-kx+\frac{\theta}{2}\right)+(A-B)^2\sin^2\left(-kx+\frac{\theta}{2}\right)} \tag{5}$$

When the reflecting boundary is solid, the incident and reflected amplitudes are equal (Reynolds, 1980), thus $A = B$.

Furthermore, if the incident and reflected waves are in phase, $\theta = 0$.

Therefore, the amplitude of the standing wave, from Eq. 5, becomes

$$|p(x,t)| = 2A\sqrt{\cos^2 kx} \tag{6}$$

The case studied in this research has an energy source at the free boundary of the fluidized bed ($x = h$), thus the pressure there becomes

$$p(h,t) = P_{fs} \cos \omega t \tag{7}$$

where P_{fs} is the source amplitude. The coefficient A can be determined by substituting P_{fs} in Eq. 6. Thus, the pressure distribution becomes

$$p(x,t) = P_{fs}\sqrt{\frac{\cos^2 kx}{\cos^2 kh}} \cos \omega t \tag{8}$$

with an amplitude

$$|p(x,t)| = P_{fs}\sqrt{\frac{\cos^2 kx}{\cos^2 kh}} \tag{9}$$

The quantity $p(x,t)$ is an even function and positive values are used thereafter.

A characteristic of the described model is that $p(x,t)$ be-

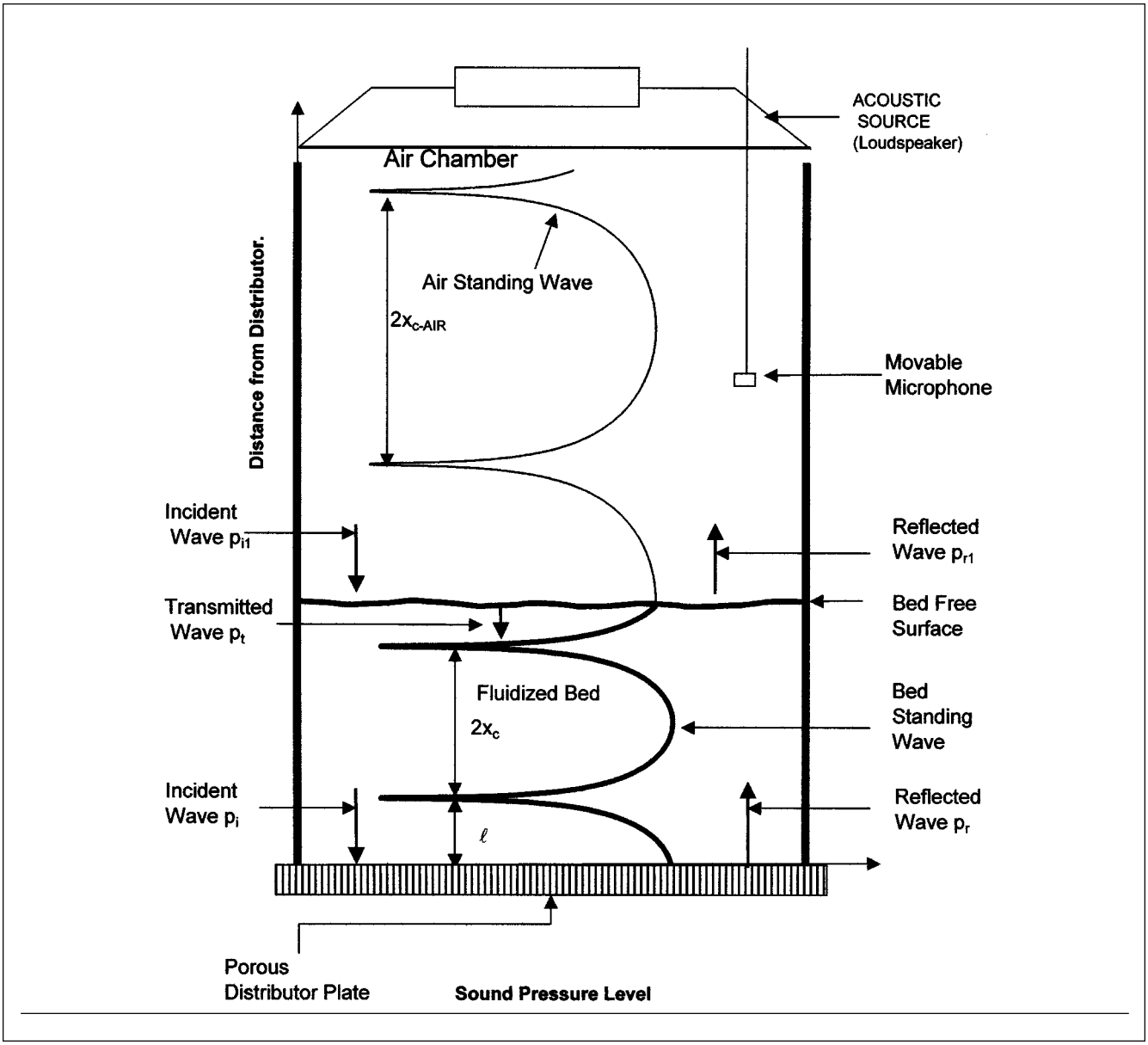

Figure 2. Acoustic scheme of the experiments.

comes very large when $\cos(kh) = 0$, which occurs at

$$kh = (2n-1)\frac{\pi}{2} \quad \text{for } n = 1, 2, \ldots. \tag{10}$$

The resonant state is reached at this condition. In reality, some energy will be dissipated and the pressure remains finite at all times.

In summary, the sound-pressure amplitude depends on the wave number, k, distance between the rigid surface and the source, h, and on the source-pressure amplitude, P_{fs}. The source amplitude is frequently expressed in decibels and is referred to as SPL_{fs}, which indicates the sound-pressure level at the free surface of the fluidized bed. See the Appendix for the SPL definition. Figure 3 shows a mechanical configuration of the fluidized-bed system and its corresponding pressure-amplitude graphs from Eq. 9 for different conditions of kh, fixed sound source distance from the distributor, h, and fixed SPL_{fs}. The piston oscillates producing the incident, p_i, and reflected, p_r, sound-pressure waves. In the curve for $kh \sim \pi/2$ the trough is slightly shifted below the free surface, and the sound-pressure magnitude is the largest. Incidentally, the sound pressure for $kh = \pi/2$ (not shown) is infinitely large, and this occurs when the trough is exactly at a distance, h, from the distributor. Increasing kh, the trough is moved toward the distributor plate and the sound-pressure level diminishes. For $kh > \pi/2$, the trough is well inside the bed, and the sound pressure is clearly lower than that for $kh \sim \pi/2$. The lowest sound-pressure levels occur at $kh = \pi$ where the sound pressures at the source and distributor plate are equal; thereafter, the sound pressures increase as kh is reduced. Figure 3 also compares the sound-pressure level for $kh < \pi/2$. The first trough cannot be seen for $kh < \pi/2$ since it would appear above the bed free surface. The sound-pressure level at the distributor plate reaches a maximum at $kh = \pi/2$ and a minimum at $kh = \pi$.

For other kh values, the sound-pressure level varies harmonically between both limits, and it is symmetric with respect to the nodes and antinodes. Figure 3 gives an example of two cases that have the same sound-pressure level at the distributor plate, SPL_o, and different kh. The troughs of each curve are located at equal distances from the sound source, but in opposite directions. This is due to the harmonic behavior with respect to kh. The kh effect is substantial on the pressure magnitude and distribution inside the medium.

Figure 4 shows the sound-pressure level at the distributor plate as a function of kh. At $(2n-1)\pi/2$, resonance is obtained. The curve was generated for the fixed sound-pressure level at the free surface.

Speed of sound in fluidized beds

Another useful relationship is provided by the minima in the standing waves. The first minimum of Eq. 5 yields the

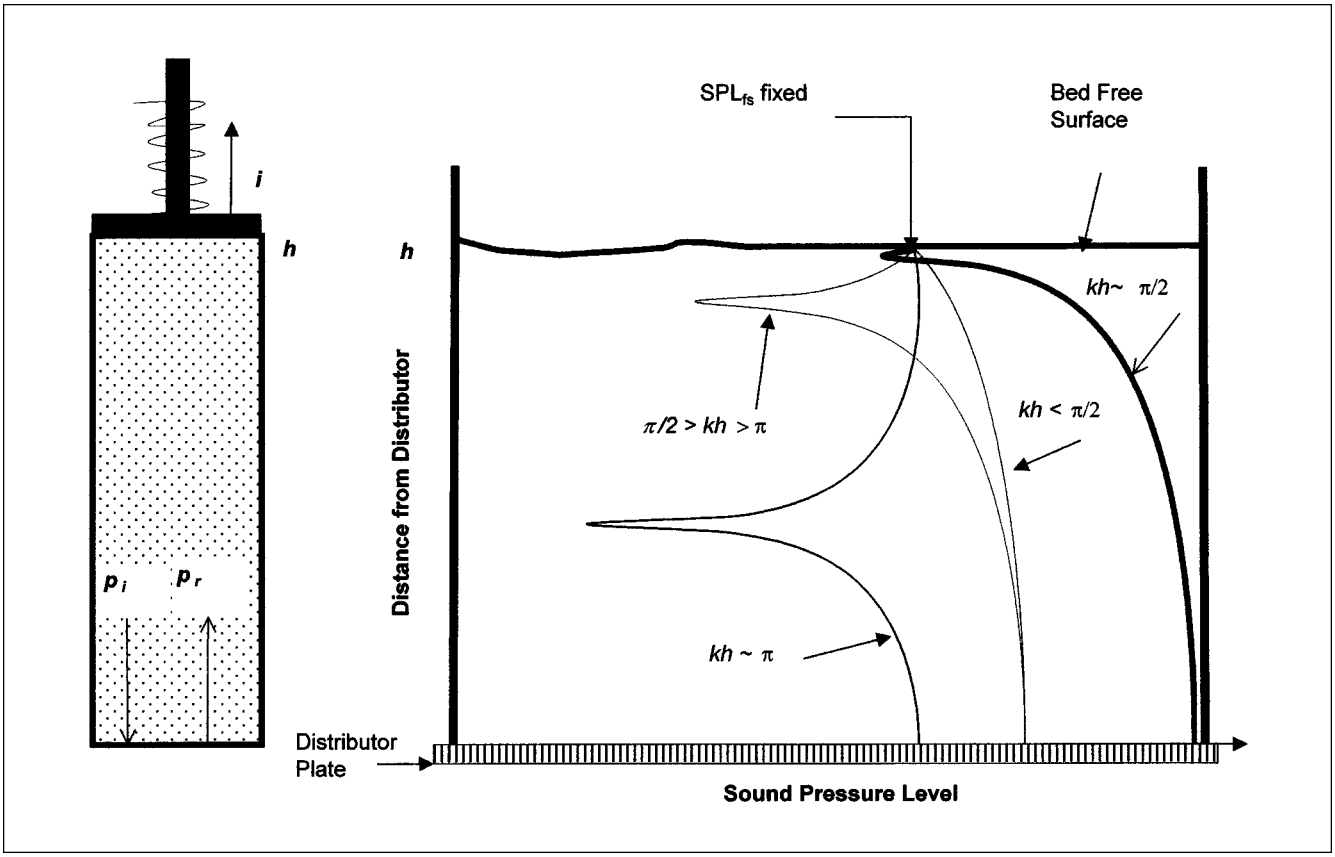

Figure 3. Sound-pressure-level distribution around the first mode of resonance for a fixed-distance from the distributer (Eq. 9).

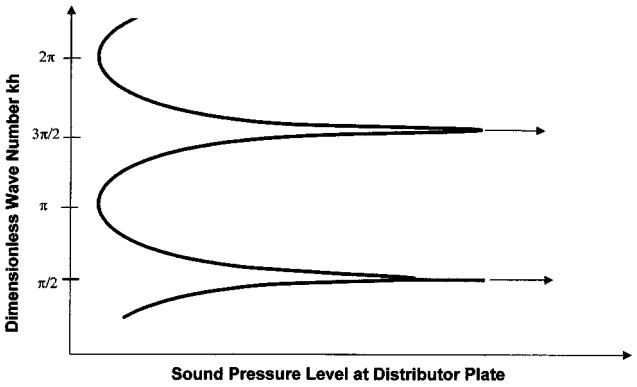

Figure 4. Sound-pressure level at distributer SPL_0 as a function of *kh* (Eq. 9).

following expression

$$c + \frac{4\pi fl}{\theta + \pi} \tag{11}$$

where l is the distance from the reflecting rigid surface to the first minimum of the standing-wave pattern, and f is the sound frequency (Hz).

Equation 11 provides a method to determine the speed of the sound in fluidized beds having a standing-wave pattern and rigid distributors. Further analysis on speed of sound, using this method, can be found in Herrera (2000).

Resonant state

Once the standing-wave pattern and speed of sound are determined, the resonance frequency, f_c, for a bed depth, h, can be computed from Eqs. 10 and 11

$$f_c = \frac{(2n-1)}{4}\frac{c}{h} \quad n = 1, 2, \ldots. \tag{12}$$

For the first mode, this is

$$f_c = \frac{c}{4h} \tag{13}$$

Assuming constant speed of sound, Eq. 13 indicates that the resonant frequency is inversely proportional to the distance between the source (the free surface, in this case) and the rigid boundary (distributor plate). In other words, the resonant frequency is proportional to the speed of sound and inversely proportional to the bed depth. In dimensionless terms, Eq. 13 can be rewritten as

$$kh = \frac{\pi}{2}$$

The resonance state has very important practical applications, since the highest pressure level is useful for better fluidization. Operating at resonant conditions has the advantage of obtaining maximum pressure, maximum particle vibrational velocity, and maximum displacement of the solid particles in the bed. Moreover, the resonant state offers an ideal situation for achieving a maximum sound-pressure level with a minimum source amplitude at the free surface.

Acoustic attenuation in fluidized beds

The attenuation, α, is an acoustic property of the medium that depends on the sound frequency. Attenuation affects the sound-pressure level distribution.

Attenuation can be included in the standard analysis of standing waves as follows

$$p(x,t) = Ae^{\alpha x}e^{j(\omega t + kx)} + Ae^{-\alpha x}e^{j(\omega t - kx)} \tag{14}$$

where α is the attenuation coefficient.

The corresponding amplitude of the last equation is (Kinsler and Frey, 1962)

$$|p(x,t)| = 2A[\cosh^2 \alpha x \cos^2 kx + \sinh^2 \alpha x \sin^2 kx]^{1/2} \tag{15}$$

and the nodal points of minimum pressure can be shown to be at

$$kx = (2n-1)\frac{\pi}{2} \quad n = 1, 2, 3, \ldots.$$

Thus, the minimum pressure becomes

$$p_{\min} = 2A \sinh(\alpha x) \approx 2A(\alpha x) \tag{16}$$

where the $\approx$ is valid for small attenuation and short distances.

Similarly, the nodal points of maximum pressure are

$$kx = n\pi \quad n = 0, 1, 2, \ldots..$$

.

Thus, the maximum pressure becomes

$$p_{\max} = 2A \cosh(\alpha x) \approx 2A(1 + \alpha^2 x^2)^{1/2} \tag{17}$$

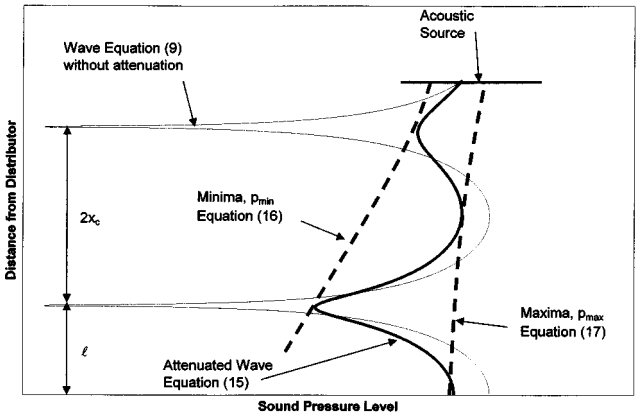

Figure 5. P_{min} and P_{max} as function of x for attenuated standing waves.

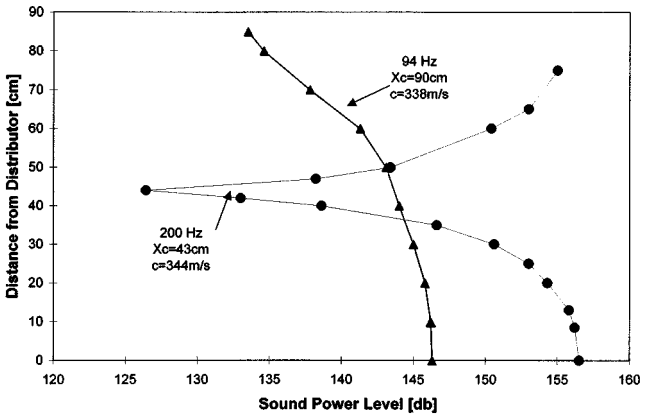

Figure 6. Standing-wave patterns in empty fluidation column.

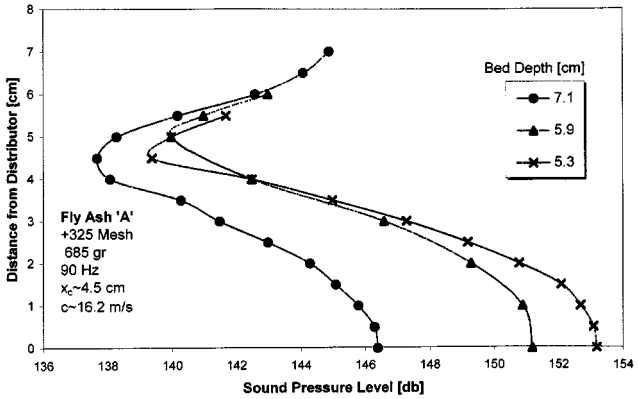

Figure 8. Experimental standing waves for fly ash "A," 90 Hz, and several bed depths.

It should be noted that $p_{\max}$ is $2A$ at the rigid boundary ($x = 0$), doubling the amplitude of the incident wave. Figure 5 illustrates $p_{\min}$ and $p_{\max}$ in attenuated standing waves using Eq. 15 and compares this to nonattenuated waves from Eq. 6. The attenuation damps out the sound-pressure intensity, thus, for the fixed free-surface condition, SPL_{fs}, the attenuated sound-pressure level at the distributor plate is lower than the nonattenuated level. However, the trough positions, which are fixed by the frequency, are the same for attenuated and nonattenuated profiles, which indicates that the critical bed depth, x_c, is independent of the attenuation, and consequently, the speed of sound is also independent of attenuation.

Experimental Results

The procedure to obtain information on the standing waves includes the measurement of the sound-pressure level at different distances from the distributor. The measurements were performed directly by traversing a movable microphone that is inserted inside the medium, as shown in Figure 2. The phase angle, θ, and the distance, l, to the first trough can be obtained from the experiments. It is possible to determine the speed of the sound in the medium in which the standing wave is formed by knowing the sound frequency, f, phase angle, θ, and distance to the first trough, l. This can be done using Eq. 11.

Several experiments were performed, and well-defined standing waves were observed in all the experiments, as well as a zero phase angle at the rigid boundary. As a consequence, the speed of sound can be fully determined.

Figure 6 shows experimental evidence for the existence of standing waves in the empty air chamber measured with the described procedure. Results for 94-Hz and 200-Hz sound frequency are plotted in the figure. The critical depth was 90 cm for 94-Hz, thus, the speed of sound from Eq. 11, resulted in 338 m/s. Similarly, the critical depth was 43 cm for 200-Hz, giving 344 m/s for the speed of sound. These results are consistent with the well-known speed of sound in air, which is 343 m/s at 50°F (10°C). All of the experiments reported in this work were performed at ambient conditions (60°F and 70% relative humidity). The lines connecting the data points show the standing waves for each case.

Standing waves were measured in all fine-powder experiments. In order to determine the uncertainty of the standing-wave readings, a statistical analysis was performed. The sound meter was calibrated before starting tests, and it was found to be accurate to within 0.5%.

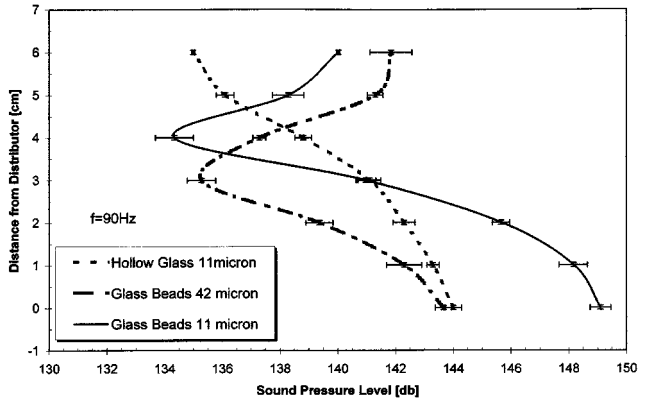

Figure 7. Uncertainty in acoustic standing-wave measurements.

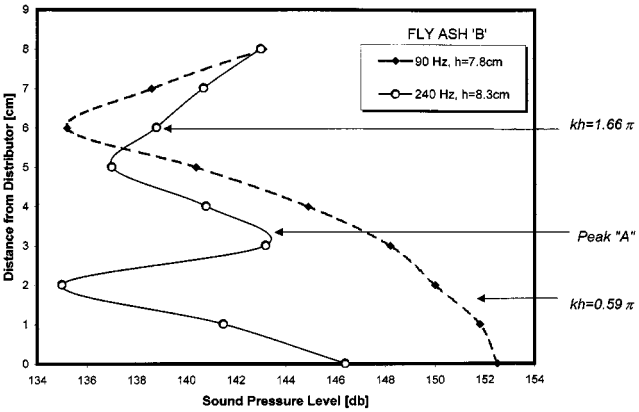

Figure 9. Effect of frequency on wave.

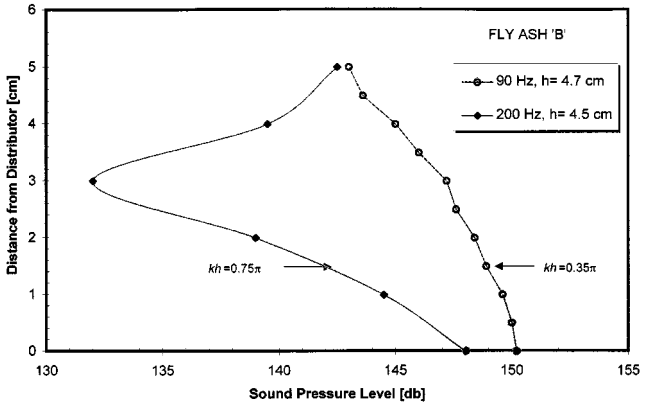

Figure 10. Effect of frequency on wave patterns.

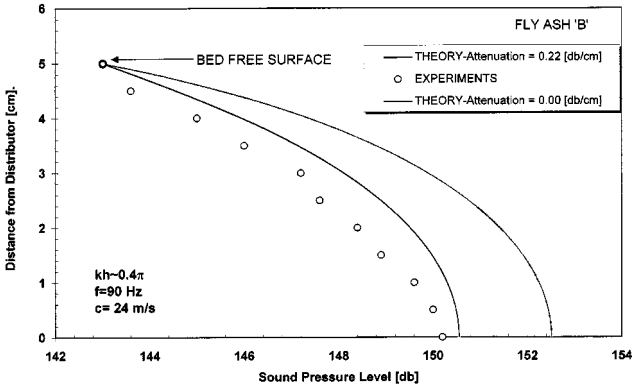

Figure 12. Standing-wave comparison for fly ash "B," $kh = 0.4\pi$.

The uncertainty of the measurements is plotted for several cases in Figure 7, using 2σ random error bars, and this shows the resulting uncertainty was less than $\pm 2\%$. The uncertainty in the readings of distance was less than $\pm 1\%$. In conclusion, this analysis indicates that the experimental results on standing-wave patterns have an uncertainty of ± 1.5 dB at the 95% confidence level.

Figures 8 through 13 show standing waves measured in fluidized beds of fly ash from two coal-fired boilers. Most of these experiments were performed for conditions near minimum bubbling, with velocities either less than, equal to, or greater than U_{MB}, depending on the experiment. No direct change in the standing-wave pattern was observed due to change in superficial gas velocity. However, gas velocity affected bed voidage and bed depth, and thus it indirectly affected the shapes of the wave patterns.

For fly ash A, the critical depth was close to 4.5 cm at 90-Hz acoustic frequency. The resulting speed of sound, obtained from Eq. 11 and from the measured waveforms, was approximately 16 m/s. Figure 8 depicts the standing-wave results with fly ash A for three different fluidized-bed depths. Standing waves appeared in all the experiments, as can be seen in the figure. Even more, the critical bed depth, the distance between the distributor and the minimum in the SPL profile, was nearly the same in all the tests, as expected for a fixed frequency. The lines connecting the data points show the standing waves for each case.

The form of the sound-pressure level profiles shown in Figure 8 are typical of distributions in fluidized beds of fine powders. Furthermore, as will be shown, the representation of standing waves is consistent with the theoretical approach developed earlier in this article.

Effect of parameter kh

The parameter kh can be varied experimentally by changing the sound frequency or changing the bed depth. Figure 9 shows the experimental results for $\pi/2 < kh < \pi$, and for $kh > 3\pi/2$. The marked points represent the experimental values and the connecting lines represent the trend curves followed by the data. For $kh = 1.66\pi$, the appearance of two "peaks" and two "troughs" can be deduced from the trend line. The peak A in the trend curve corresponds with the predicted peak from Eq. 9, which appears for $\pi < kh < 3\pi/2$. Thus, this observation is consistent with the theory. For $kh = 0.59\pi$ the trend curve suggests the appearance of a unique peak formed at the distributor plate and a unique trough formed at around 6 cm from the distributor plate.

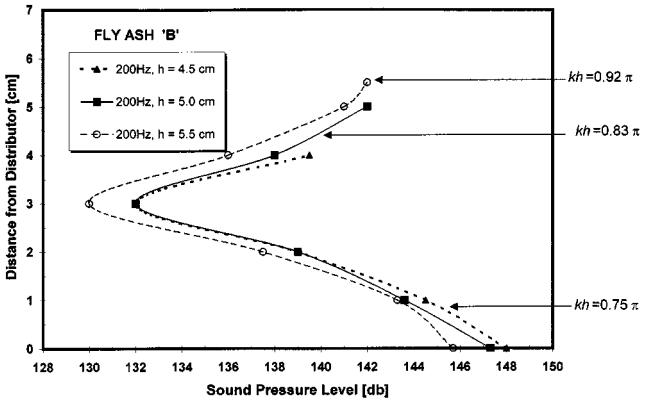

Figure 11. Effect of bed depth on wave patterns.

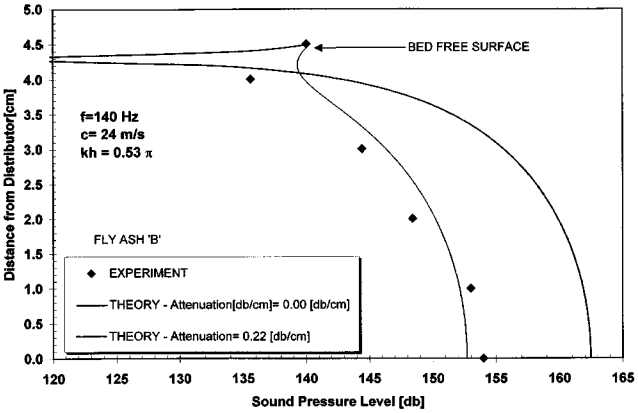

Figure 13. Standing-wave comparison for fly ash "B," $kh = 0.53\pi$.

The experimental results for $\pi/2 < kh < \pi$, and $kh < \pi/2$, are presented in Figure 10. In these experiments kh changes were obtained through frequency variations, and the bed depth was kept relatively constant. The marked points represent the experimental values and the connecting lines represent the trend curves followed by the data. As expected from Eq. 9, a trough first appears at $kh = 0.5\pi$, when the first node and resonance conditions are reached. The trend line for $kh = 0.35\pi$ shows no evidence of a trough. It also shows a continuous increase of sound-pressure-level amplitude from the free surface. However, for $kh = 0.75\pi$, the trend curve shows that a trough is visible around 3 cm from the distributor plate. Therefore, these results are consistent with the theoretical predictions for the sound-pressure-level pattern.

Alternatively, variations in kh were obtained experimentally through bed-depth changes with fixed frequency. Results for fly ash B are presented in Figure 11, where the frequency was fixed at 200 Hz for all the tests. The marked points represent the experimental values and the connecting lines represent the trend curves followed by the data. The trend curves show that a trough appears approximately 3 cm from the distributor plate. It also shows that it is similar in all the experiments. From the theoretical point of view (Eq. 9), troughs are defined by the frequency and the speed of sound of the medium. Therefore, since the frequency and the speed of sound are fixed, the observed trend is consistent with theoretical considerations. Another observation is the increase of sound pressure level, SPL_o, as kh is reduced from 0.92π to 0.75π. This behavior can also be predicted from theoretical considerations, since the sound pressure increases, as kh is closer to $\pi/2$, which is the value for the resonant configuration.

A comparative study of the sound-pressure level distribution was carried out to validate the model. For that purpose, theoretical predictions and experimental results are compared for typical cases in Figures 12, 13, and 14. According to Eqs. 9 and 15, which describe the undamped and damped models, the most relevant parameter is kh, thus, the comparative analysis considered its effect on the sound-pressure level. Values for the attenuation coefficients used in Figures 12 to 14 were calculated from the measured waveforms.

For a system with $kh \leq \pi/2$, as depicted in Figure 12, the results show a continuous pressure increase from the free surface. These results are compared with the theoretical prediction using the undamped model from Eq. 9 and damped model from Eq. 15. Although the undamped model (attenuation = 0.0 dB/cm) overpredicts the sound-pressure level, the trending is reasonable. The attenuation model corrects the difference between theoretical prediction and experiments. More information on attenuation coefficient is found in Herrera (2000).

The results for $kh = 0.53\pi$ are plotted in Figure 13. The undamped prediction from Eq. 9 is unrealistic, and the quantitative difference between the theoretical and experimental sound-pressure level is considerable. A possible explanation for this large difference can be the fact that the undamped model becomes more and more unrealistic as the bed depth approaches the resonance condition. The resonance condition is reached at $kh = \pi/2$, when the theoretical sound pressure is infinitely large due to the zero value of the denominator in Eq. 9. Figure 13 also shows theoretical results with attenuation included in the model. Consequently, as shown by the figure, the predicted sound-pressure level becomes much more realistic when attenuation is included.

Figure 14 depicts the results for $kh = 0.83\pi$. The sound-pressure magnitude increases from 3 cm to 4 cm from the distributor plate, indicating the presence of a trough located around 3 cm from the distributor. From the theoretical point of view the attenuation effect at the trough is significant. However, its effect at the distributor plate is slight. The results show that the theory is able to predict the sound pressure for kh near π, and both the undamped and damped models give similar predictions at the distributor plate.

Although the theory is able to explain standing-wave formation, there are still some issues the model is not able to predict satisfactorily. For example, the sound pressure at the distributor plate is sometimes higher than ideally expected. The attenuation parameter cannot explain this difference, but uncertainties in the sound measurements, which are around 1.5 dB, as was discussed before, may be the cause of the differences. Finally, it should be pointed out that while the validity of the model was tested with frequencies ranging from 90 Hz to 200 Hz, the results shown here are for a narrow range of bed depths. Additional experiments would need to be run with much deeper beds to fully validate the model.

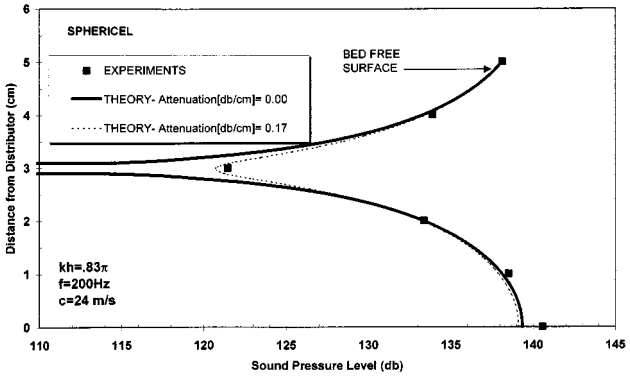

Figure 14. Standing-wave comparison for Sphericel, $kh = 0.83\pi$.

Conclusions

A theoretical model is proposed to predict the sound-pressure distribution inside fluidized beds. The model is based on classical acoustic theory, where the fluidized bed medium behaves as a one-dimensional quasi fluid.

In the cylindrical configuration modeled in this research, the sound is treated as traveling in a pipe. The pipe is closed at one end, and it has a harmonic power source at the other end. Accordingly, a standing wave appears along the length of the bed and the theory developed in this section can predict the behavior of the sound waves inside the bed.

This model also provides a method to compute the speed of sound for fluidized beds, based on standing-wave theory. In addition, it was possible to determine the natural frequency of the system. This is proportional to the speed of the sound of the bed and inversely proportional to the bed depth.

The highest sound-pressure level in the bed occurs at this resonance condition.

A set of experiments showing fluidized-bed standing waves was presented. Standing waves were found in all the experiments, and they served to formulate the problem and provide information on the bed speed of sound and acoustic attenuation.

It was found that bed bubbling, instead of spouting and channeling, was achieved at higher sound-pressure levels. The harmonic nature of this process includes the possibility of a resonant state, with the highest-pressure level occurring at resonance. The resonant bed depth occurs at $(2n-1)$ bed quarter-wavelengths, which in dimensionless terms is equivalent to $kh \sim \pi/2$, where k is the bed wave number and h is the bed depth.

The theory of acoustic-wave propagation, restricted to a one-dimensional., single-phase medium, was able to explain the experiments. Its application is limited to weak waves with small amplitudes, negligible gas flow rate, and speed of sound larger than the particle velocity.

Notation

A = constant of integration
c = speed of sound, m/s
d_p = mean particle size
f = sound frequency, Hz
f_c = resonance frequency
h = bed depth, cm
$k = 2\pi f/c$ wave number
$k_0 = k + j\alpha(\omega)$ = the complex wave number
kx = dimensionless wave number
l = distance from distributor plate to the first standing-wave trough
L_w = Lifshitz–van der Waals constant
p = pressure
p_{fs} = sound-pressure amplitude at free surface
$p_{\max}$ = maximum pressure
$p_{\min}$ = minimum pressure
P = absolute magnitude of the sound pressure
P = hydrostatic pressure
P_{ref} = the reference pressure, $p_{\text{ref}} = 2\times10^{-5}$ Pa
$p_{rms}(x)$ = sound-pressure root mean square
SPL = sound-pressure level, dB
SPL_{fs} = sound-pressure level at the free surface
SPL_o = sound-pressure level at the distributor plate
U_{MB} = minimum bubbling velocity
V = volume
x = distance from distributor
x_c = distance between a node (maximum or crest) and an antinode (minimum or trough)
z = distance of separation between interacting spheres

Greek letters

α = attenuation factor
ϵ = void fraction
λ = wavelength, $\lambda = c/f$
θ = phase angle
ω = angular frequency, $\omega = 2\pi f$

Subscripts

fs = free surface
g = gas phases
i = incident
o = distributor plate
p = particle
r = reflected
T = total

Literature Cited

Abrahamsen, A., and D. Geldart, "Behaviour of Gas-Fluidized Beds of Fine Powders Part I. Homogeneous Expansion," *Powder Technol.*, **26**, 35 (1980).

Arnaldos, J., J. Casal, A. Lucas, and L. Puigjaner, "Magnetically Stabilized Fluidization: Modelling and Application to Mixtures," *Powder Technol.*, **44**, 1, 57 (1985).

Beeckmans, J., and J. Chu, "Solids Mixing Kinetics and Segregation in a Vibrostatilized Fluid Bed," *Can. J. Chem. Eng.*, **65**(4), 536 (1987).

Beranek, L., *Acoustics*, Acoustic Society of America, Melville, NY (1996).

Chirone, R., and L. Massimila, "Sound Assisted Aeration of Beds of Cohesive Solids," *Chem. Eng. Sci.*, **49**(8), 1185 (1994).

Chirone, R., and P. Russo, "Resonant Behavior of Cluster-Subcluster Structures in Sound Assisted Fluidized Beds," *Proc. Int. Symp. Engineering Foundation, Fluidization VIII*, Tours France (1995).

Chirone, R., L. Massimila, and S. Russo, "Bubble-Free Fluidization of a Cohesive Powder in an Acoustic Field," *Chem. Eng. Sci.*, **48**(1), 41 (1993).

Chirone, R., L. Massimila, and S. Russo, "Bubbling Fluidization of a Cohesive Powder in an Acoustic Field," *Fluidization VII, Proc. Engineering Foundation Conf. on Fluidization*, New York Engineering Foundation, p. 545 (1992).

Geldart, D., "Types of Gas Fluidization," *Powder Technol.*, **7**, 285 (1973).

Herrera, C., "Acoustic Characteristics of Fine Powder Fluidized Beds," PhD Thesis, Lehigh University, Bethlehem, PA (2000).

Herrera, C., and E. Levy, "Characteristics of Acoustic Standing Waves in Fluidized Beds," *Proc. American Institute of Chemical Engineers*, Dallas, TX (1999).

Jaraiz, M., O. Levenspiel, and T. Fitzerald, "The Uses of Magnetic Fields in the Processing of Solids," *Chem. Eng. Sci.*, **38**(1), 107 (1983).

Kinsler, L. E., and A. R. Frey, *Fundamentals of Acoustics*, Wiley, New York (1962).

Levy, E., C. Herrera, and T. Masaki, "Bubbling Fluidization of Fine Powders in a High Intensity Acoustic Field," *Proc. Int. Conf. on Fluidization*, Engineering Foundation, New York (1998).

Levy, E., C. Herrera, M. Coates, and R. Afonso, "Beneficiation of Fly Ash Using a Fluidized Bed Separator," *Proc. Int. Symp. on Management and Use of CCPS*, American Coal Ash Association, FL (1999).

Malhotra, K., L. Law-Kwet-Cheong, and A. Mujumdar, "Pressure-Drop Charcterization for Vibrated Beds of Dry and Sticky Particles," *Powder Technol.*, **39**, 101 (1984).

Massimila, L., G. Volpicelli, and G. Raso, "A Study on Pulsing Gas Fluidization of Beds of Particles," *Chem. Eng. Symp. Ser.*, **62**, 63 (1966).

Morse, P., and U. Ingard, *Theoretical Acoustics*, Princeton Univ. Press, Princeton, NJ (1986).

Morse, R., "Sonic Energy in Granular Solid Fluidization," *Ind. Eng. Chem.*, **47**, 1170 (1955).

Nowak, W., M. Hasatani, and M. Derczynski, "Fluidization and Heat Transfer of Fine Particles in an Acoustic Field," *AIChE Symp. Ser.*, 137 (1993).

Reynolds, D., *Engineering Principles of Acoustics*, Allyn & Bacon, Boston (1981).

Appendix

Root mean square

The root mean square of sound, p_{rms}, is the overall measurement of the amplitude of the sound pressure defined by

$$p_{rms} = \frac{|p(x,t)|}{\sqrt{2}} = \frac{P}{\sqrt{2}}$$

where P is the absolute magnitude of the sound pressure, $P = |p(x,t)|$.

Sound-pressure level

The sound-pressure level is the amplitude of acoustic pressure compressed to a logarithmic scale and referred to the threshold of human hearing, defined by

$$\mathrm{SPL} = 20\log\left[\frac{p_{rms}}{P_{\mathrm{ref}}}\right]$$

where P_{ref}, the reference pressure, is typically chosen to be the value at the threshold of human hearing, that is, $p_{\mathrm{ref}} = 2 * 10^{-5}$ Pa.

Manuscript received July 31, 2000, and revision recieved Aug. 20, 2001.